2624 Vol. 34, No. 12 / December 2017 / Journal of the Optical Society of America B Research Article

Journal of the Optical Society of America B OPTICAL PHYSICS

Enhanced transmission via cavity modes in gratings formed by subwavelength metallic cylinders

Marcelo Lester[1,*] and Diana C. Skigin[2,3]

[1]Instituto de Física Arroyo Seco, IFAS (UNCPBA) and CIFICEN (UNCPBA-CICPBA-CONICET), Grupo Óptica de Sólidos–Elfo, Pinto 399, 7000 Tandil, Argentina
[2]Universidad de Buenos Aires, Facultad de Ciencias Exactas y Naturales, Departamento de Física, Grupo de Electromagnetismo Aplicado, Buenos Aires, Argentina
[3]CONICET–Universidad de Buenos Aires, Instituto de Física de Buenos Aires (IFIBA), Buenos Aires, Argentina
*Corresponding author: mlester@exa.unicen.edu.ar

Received 1 September 2017; revised 25 October 2017; accepted 25 October 2017; posted 27 October 2017 (Doc. ID 306073); published 27 November 2017

In the last few decades, special attention has been paid to the optical response of structures composed of periodic subwavelength slits in thin metallic sheets. Extraordinary transmission and evanescent-to-propagating conversion are two of the main effects that have been most investigated in these systems. In this paper, we present an alternative way of enhancing the intensity diffracted by a grating through morphological electromagnetic resonances. Unlike nanoslit arrays, in this system the cavities are formed by periodically distributed chains of metallic subwavelength cylinders, which behave like walls that confine the fields and thus show resonant behavior. The set of cavities is illuminated by an evanescent wave generated by total internal reflection. We show that resonant coupling of cavity modes excited by the inhomogeneous wave produces enhanced transmission of up to 92% and also that the system has the ability of steering most of the transmitted intensity in a particular direction given by the diffraction orders. The results are compared with those obtained from a similar structure formed by periodically distributed perfectly conducting solid walls.

OCIS codes: (050.6624) Subwavelength structures; (290.0290) Scattering; (050.0050) Diffraction and gratings; (050.2230) Fabry-Perot.

https://doi.org/10.1364/JOSAB.34.002624

1. INTRODUCTION

A large variety of electromagnetic effects are produced by resonant coupling between incident radiation and different eigenmodes supported by a metallic structure with subwavelength characteristics. Resonant mechanisms such as Fabry–Perot resonances, surface plasmon excitation, Wood–Rayleigh anomalies, phase resonances, and grating resonances produce remarkable features in their transmitted responses [1–11]. Metamaterials, and, more recently, metasurfaces, have been extensively investigated in order to optimize the coupling between the electromagnetic field and their subwavelength features to achieve different properties [12–14]. Combination of different resonant mechanisms has also been employed as a means to improve the coupling efficiency and, consequently, the performance of the structure for a particular response such as enhanced transmission [1,3]. Only a few authors reported that the coupling between the light and the resonances of a periodic structure can be significantly improved using an evanescent wave [15]. Despite the growing interest in these phenomena and in their derived applications, most of the studies investigate the response of the system under propagating incidence.

On the other hand, interest in the study of physical mechanisms that produce evanescent-to-propagating wave conversion by means of diffractive devices with subwavelength features has also increased in the past few years. These studies are prompted by the interest in the possibility of generating optical images with details much smaller than the operating wavelength, and enabled the development of near-field superlenses and hyperlenses [16], which convert evanescent into propagating waves and can achieve resolutions below $\lambda/5$ [17,18].

In previous works, we have reported evanescent-to-propagating wave conversion by means of a periodic array of wires near a dielectric interface at which evanescent waves are generated. We have shown that the transmitted intensity can be increased by means of Fabry–Perot resonances within the subwavelength slits [19,20] and by excitation of eigenmodes within the gap between the array and the interface (p polarization) [21]. We have

also explored the performance of a periodic array of cylinder chains, which converts evanescent into propagating waves and can steer the transmitted beam into a predetermined direction, which can be tailored by appropriate choice of geometrical parameters of the structure [22]. Excitation of cavity modes as a mechanism to produce transmission enhancement has been widely investigated for 1D structures with subwavelength slits [23–25]. However, not many authors studied the case of wider cavities, i.e., with widths comparable to the incident wavelength [8,26].

Motivated by recent advances in super-resolution techniques, in this paper we numerically demonstrate a novel and efficient way of evanescent-to-propagating wave conversion, with optimized transmission and controllable directionality. The proposed physical mechanism is the excitation of resonances within the cavities formed between the chains of subwavelength cylinders arranged in a periodic structure. Unlike the plasmon amplification mechanism, in this structure the evanescent waves are amplified via morphological resonances, which provide more degrees of freedom for the system design. This intensification mechanism is independent of the material of the periodic structure, the incident wavelength, and, to some extent, its polarization. This structure could be employed for super-resolution systems, which rescue high-resolution information and collect it in the far field.

The paper is organized as follows: in Section 2, we present the systems under study and briefly outline the numerical methods used to address each of the scattering problems. In Section 3, the results obtained for different configurations of the system are presented, including the case of an isolated chain, of two chains (a single cavity), and of a larger array comprising several cavities. We analyze the resonant behavior of the structure by computing the far and near fields, and study the dependency of the transmission enhancement on the number of chains, the distance between adjacent cylinders, and the total height of the chains. To better understand the physical mechanisms involved in the interaction of evanescent waves with this system, we compare the results with those corresponding to a similar but simplified problem: an infinitely periodic structure in which the wire chains are replaced with solid perfectly conducting wires of rectangular cross section. Also in this case, far- and near-field plots are presented, which permit a deeper physical insight on the addressed phenomenon. Finally, concluding remarks are given in Section 4.

2. CONFIGURATION AND METHODS

We consider a finite structure formed by equally spaced chains of subwavelength wires. To solve the scattering problem with this system, we employ the integral method. We also compare the results obtained with those of a periodic grating formed by rectangular perfectly conducting wires, and use the modal method to solve this problem. Therefore, in this section we present both configurations and briefly summarize the methods employed in each case.

A. Finite Array of Subwavelength Wires

The system under study is a finite array of equally spaced chains formed by cylindrical metallic wires in vacuum, such that the space between adjacent chains can be regarded as a cavity. In this way, the structure forms a finite grating of period d and height h, as shown in Fig. 1(a). The array is separated by a distance e from the interface between region 1 (ϵ_1) and region 2 (ϵ_0) (all media are non-magnetic). The chains are formed by a pile of n metallic wires of circular cross section. Each wire has a diameter c and a dielectric permittivity ϵ, and the distance between the centers of adjacent wires within the same chain is a. The structure is illuminated from medium 1 by a p- or s-polarized Gaussian beam of width W and wavelength λ in vacuum, which forms an angle θ_0 with y axis.

The general integral formalism is based on both Green and extinction theorems [19,27–29]. For systems with translational symmetry and the incidence wavevector contained in the (x, y) plane (2D systems), the expressions for the scattered field in each medium are

$$\phi_\alpha^{(0)}(\mathbf{r}) = \phi_\alpha^{(\mathrm{inc})}(\mathbf{r}) + \sum_{j=1}^{N} \times \left\{ \frac{i}{4} \int_{C_j^{(+)}} \mathrm{d}l' \times \left[\frac{\partial H_0^{(1)}\left(\sqrt{\epsilon_0} k_0 |\mathbf{r} - \mathbf{r}'|\right)}{\partial \mathbf{n}'} \phi_\alpha^{(0)}(\mathbf{r}') \right] - \left[H_0^{(1)}\left(\sqrt{\epsilon_0} k_0 |\mathbf{r} - \mathbf{r}'|\right) \frac{\partial \phi_\alpha^{(0)}(\mathbf{r}')}{\partial \mathbf{n}'} \right] \right\}, \tag{1}$$

$$\phi_\alpha^{(j)}(\mathbf{r}) = -\frac{i}{4} \int_{C_j^{(-)}} \mathrm{d}l' \left[\frac{\partial H_0^{(1)}\left(\sqrt{\epsilon_1} k_0 |\mathbf{r} - \mathbf{r}'|\right)}{\partial \mathbf{n}'} \phi_\alpha^{(j)}(\mathbf{r}') - H_0^{(1)}\left(\sqrt{\epsilon} k_0 |\mathbf{r} - \mathbf{r}'|\right) \frac{\partial \phi_\alpha^{(j)}(\mathbf{r}')}{\partial \mathbf{n}'} \right], \tag{2}$$

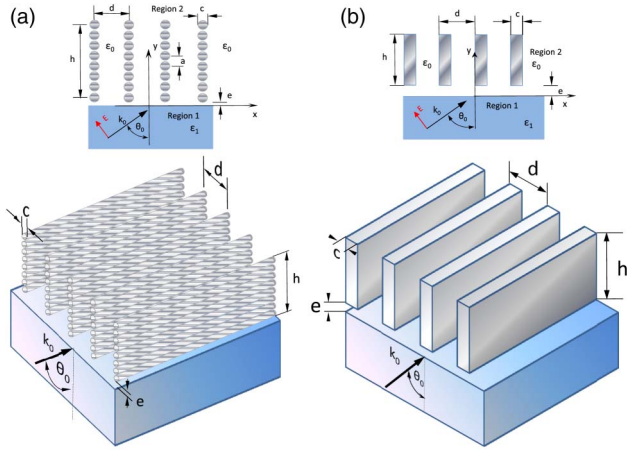

Fig. 1. Systems under study and the configuration of the scattering problem. (a) Finite array of metallic subwavelength cylinder chains illuminated by a Gaussian beam, which comes from a dielectric medium with an angle θ_0 larger than the critical angle for the interface between the incidence and transmission media. The geometrical parameters are indicated. Inset: planar view of the scattering configuration. (b) Simplified system: infinitely periodic array of perfectly conducting rectangular wires illuminated by a plane wave under total internal reflection conditions. The geometrical parameters are indicated. Inset: planar view.

for $j = 1, \ldots N$, where $\phi_\alpha^{(j)}(\mathbf{r})$ represents the complex amplitudes of the electric ($\alpha = s$) or magnetic ($\alpha = p$) field in the host medium ($j = 0$), or within any of the N scatterers ($j = 1, \ldots, N$). dl' is a differential element of line over the contour C_j. The superscript (+) in $C_j^{(+)}$ represents the cross-section contour of the jth scatterer when $\mathbf{r}'$ tends to C_j from the host medium, and in this case $\mathbf{n}'$ (the versor normal to this contour) points toward the interior of the jth medium. Conversely, $C_j^{(-)}$ represents the cross-section contour of the jth scatterer when $\mathbf{r}'$ tends to C_j from the interior of the jth medium, and $\mathbf{n}'$ points outwards of the jth medium. $H_0^{(1)}$ is the first-class zero-order Hankel function.

In 2D problems, the boundary conditions reduce to two separate scalar equations for each polarization mode –s (electric field perpendicular to the plane of incidence) and p (electric field contained in the plane of incidence):

$$[\phi_\alpha^{(0)}(\mathbf{r})]_{\mathbf{r}\in C_j^{(+)}} = [\phi_\alpha^{(j)}(\mathbf{r})]_{\mathbf{r}\in C_j^{(-)}}, \tag{3}$$

$$\left[\frac{\partial\phi_\alpha^{(0)}(\mathbf{r})}{\partial n'}\right]_{\mathbf{r}\in C_j^{(+)}} = \left[\eta_j(\alpha)\frac{\partial\phi_\alpha^{(j)}(\mathbf{r})}{\partial n'}\right]_{\mathbf{r}\in C_j^{(-)}}, \tag{4}$$

with $\eta_j(s) = 1$ and $\eta_j(p) = \epsilon/\epsilon_0$ (we consider identical cylinders of dielectric permittivity ϵ). To compute the far field, we make use of the asymptotic expression of the Hankel functions when $|\mathbf{r} - \mathbf{r}'| \to \infty$, and substitute it in the previous equations:

$$\phi_\alpha^{(\mathrm{scatt})}(r,\theta) = \frac{\exp\left[i\sqrt{\epsilon_0}k_0 r - \pi/4\right]}{\sqrt{8\pi(\epsilon_0)^{1/2}k_0 r}} \times \sum_{j=1}^{N}\left\{\int_{C_j^{(+)}} \mathrm{d}l'\left((\mathbf{n}'\cdot\mathbf{k}_{\mathrm{scatt}})\phi_\alpha^{(0)}(\mathbf{r}') - i\frac{\partial\phi_\alpha^{(0)}(\mathbf{r}')}{\partial\mathbf{n}'}\right) \times \exp(-i\mathbf{k}_{\mathrm{scatt}}\cdot\mathbf{r})\right\}, \tag{5}$$

where $\mathbf{k}_{\mathrm{scatt}}$ is the propagation vector defined as

$$\mathbf{k}_{\mathrm{scatt}} = \sqrt{\epsilon_0}k_0(\sin\theta, \cos\theta, 0), \tag{6}$$

and θ is the observation angle. Then, the reflected field corresponds to $-90° < \theta \leq 90°$ and the transmitted field corresponds to $90° < \theta \leq 270°$.

B. Simplified Model: Periodic Array of Rectangular Wires

As is well known, an array of closely spaced cylinders performs very similarly to a flat metallic slab [30]. Consequently, in order to better interpret the results obtained for the system of cylinder chains, we compare them with those of an infinitely periodic grating formed by regularly spaced perfectly conducting wires of rectangular cross section, as shown in Fig. 1(b). The period of the structure is d and the wires have a rectangular cross section of side c and height h. The system is illuminated by a plane wave of wavelength λ in vacuum, forming an angle θ_0 with y axis. The array of wires is at a distance e from a dielectric interface, which separates the incidence dielectric medium (ϵ_1) from the wires' host medium (ϵ_0), which is set to be vacuum. Since the incident wavevector is contained in the main section of the structure, the vectorial problem can be separated into two scalar problems corresponding to the basic linear polarization modes s and p. The diffraction problem is solved separately for each polarization mode, using the modal method [21], which consists of dividing the spatial domain into regions in each of which the fields are expanded into their own eigenfunctions. At the interfaces between adjacent regions, the fields are matched by applying the boundary conditions and the resulting equations are projected into convenient bases, which lead to a matrix system for the unknown reflected and transmitted amplitudes. More details on this formulation are given in Ref. [21].

3. RESULTS

We start our analysis by studying the evolution of the transmitted response of the system as the number of chains increases. In Fig. 2, we show the total transmitted intensity

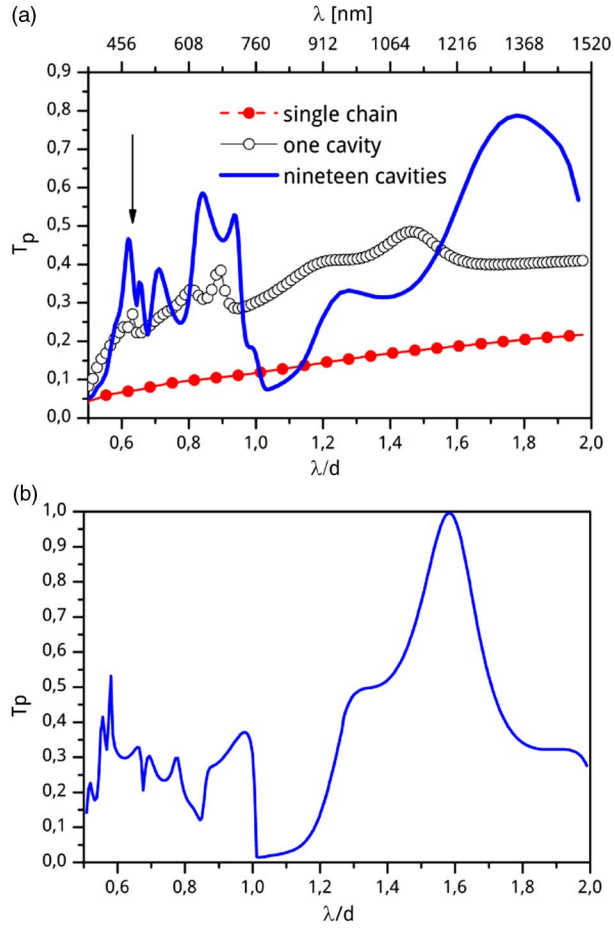

Fig. 2. Total transmission in p mode as a function of wavelength. (a) Finite array of Ag subwavelength cylinder chains with $c/d = 0.12$, $a/d = 0.125$, $h/d = 1.295$, and $e/d = 0.06$, illuminated by a Gaussian beam of half-width $W/d = 6.6$ ($d = 760$ nm). The red dashed line corresponds to a single chain comprising 10 wires. The black solid line with open circles corresponds to a structure of two chains separated by a distance d, which form an isolated cavity, and the blue solid line corresponds to 20 chains of cylinders separated a distance d from each other (19 cavities). The dielectric permittivity of Ag is taken from [31]. (b) Infinitely periodic array of rectangular perfectly conducting wires of $c/d = 0.12$, $h/d = 1.295$, and $e/d = 0.06$. In both cases, the incidence angle is $\theta_0 = 42°$, which produces evanescent waves by total internal reflection, $\nu_1 = \sqrt{\epsilon_1} = 1.52$ and $\epsilon_0 = 1$.

for p polarization (T_p) as a function of incident wavelength for (a) three different structures, namely, a single chain of cylinders (dashed line with solid red circles), two chains of cylinders (solid black line with open circles), and 20 equally spaced chains (solid blue line), and (b) an equivalent perfectly periodic structure formed by rectangular wires. For Fig. 2(a), the parameters of the structures considered are $c/d = 0.12$, $a/d = 0.125$, $h/d = 1.295$, and $e/d = 0.06$, with $d = 760$ nm. The refraction index of the incident medium is $\nu_1 = \sqrt{\epsilon_1} = 1.52$ (silica), whereas the host medium is vacuum ($\epsilon_0 = 1$), and the dielectric permittivity of Ag is taken from [31]. In Fig. 2(a), the structure is illuminated from medium 1 by a Gaussian beam of half-width $W/d = 6.6$, which is focused on the interface forming an angle $\theta_0 = 42°$, which is larger than the critical angle of $\theta_c = 41.13°$, in order to produce an evanescent wave at the interface. In the case of Fig. 2(b), the incident field is a plane wave with the same incidence angle.

As can be observed in Fig. 2(a), the transmission spectrum of the single chain is a slowly growing function, which does not show any relevant features. However, for a two-chain structure (solid line with open circles), the transmitted response retains the increasing character of the single-chain curve, but a set of peaks starts to emerge. When more chains are added to the structure, these peaks become more significant and well-defined (solid curve), and even new peaks appear, with transmission maxima that reach up to 80% for $\lambda/d = 1.8$. Taking into account that an array of closely spaced cylinders can be regarded as a flat metallic slab [30], the two-chain structure forms a single cavity, whereas the 20-chain structure forms 19 adjacent cavities. Then, the correlation between corresponding transmitted spectra becomes clear: the peaks are the result of cavity resonances that are reinforced by the addition of cavities. Besides, the addition of chains to the structure generates new peaks, which result from the coupling between the fields of adjacent cavities, and also produces an intensification of the transmitted response for certain resonant wavelengths. This is consistent with the transmittance curve for the perfectly periodic system [Fig. 2(b)], which shows a striking resemblance with the curve corresponding to 20 chains. Even though the positions of the peaks do not match perfectly, the general shapes of both curves are very similar. Taking into account that the systems have many differences (cylindrical wire chains versus solid rectangular wires, finite structure versus infinitely periodic structure, Ag versus perfect conductor, Gaussian beam versus plane wave), it is to expect that the spectral positions of the resonances would vary. However, the similarity between both curves suggests that the underlying resonant mechanism is the same for both structures.

Another interesting aspect to highlight is the interplay between Rayleigh anomalies and Bragg scattering. In a diffraction grating, a Rayleigh anomaly occurs when a particular diffraction transmitted order becomes grazing, that is, when

$$\pm 1 = \sin\theta_0\sqrt{\frac{\epsilon_1}{\epsilon_0}} \pm \frac{n}{\sqrt{\epsilon_0}}\frac{\lambda}{d} \tag{7}$$

is satisfied, with $\sin\theta_0\sqrt{\epsilon_1} \simeq 1.017$ and $\epsilon_0 = 1$ for the parameters used in this paper. When this condition holds, the total power is redistributed among the remaining propagating (reflected and transmitted) orders, and this might produce sudden variations on their efficiencies. For instance, Eq. (7) is satisfied for $n = 2$ and $\lambda/d \approx 1$ or for $n = 3$ and $\lambda/d \approx 0.67$. On the other hand, the cylinders' structure can be thought of as a 1D photonic crystal, whose planar layers are formed by chains of subwavelength cylinders separated by space gaps of width d, in which Bragg scattering takes place. The Bragg condition, given by $2(d/\lambda) = n$, determines the wavelengths at which destructive interference takes place, and, therefore, no propagation is allowed along the structure. Note that for the incidence conditions considered in the present study, the Bragg condition is approximately equal to the Rayleigh condition given by Eq. (7). Then, at these particular wavelengths, the grazing order does not propagate along the structure, and the evanescent-to-propagating conversion mechanism is modified significantly. In a perfectly periodic structure, a noticeable decrease in transmission is expected at these wavelengths, as observed in Fig. 2(b) at $\lambda/d = 1$ and $\lambda/d = 0.67$.

In Fig. 3(a), we show the magnetic field intensity ($|H|^2$) near the single-cavity structure (two adjacent chains) at the resonant peak indicated by an arrow in Fig. 2(a) ($\lambda/d = 0.64$), and compare it with the corresponding resonance for 19 cavities [20 chains, $\lambda/d = 0.651$; Fig. 3(b)], in which case the near field is only plotted in the central cavity, i.e., between the tenth and eleventh chains. We can see that both maps show very similar field distributions. Two vertical lobes are formed within the cavity in both cases, suggesting the excitation of a particular cavity mode. Note the evanescent wave coming from the left along the dielectric interface in Fig. 3(a). In what follows, we explore different resonant modes excited within the cavities formed by the cylinder chains.

In Fig. 4, we show maps of near-field intensity ($|H|^2$) at the central cavity for several resonant peaks observed in the transmission spectrum for 19 cavities [solid line in Fig. 2(a)], located

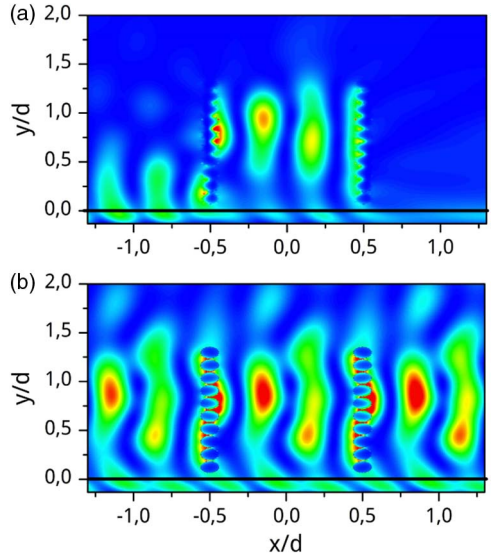

Fig. 3. $|H|^2$ in the vicinity of the structure for (a) a single cavity at $\lambda/d = 0.64$ [indicated by an arrow in Fig. 2(a)] and (b) a system formed by 20 chains (19 cavities) at $\lambda/d = 0.651$. The color scales are adapted in each plot in order to highlight the magnetic field distribution of each resonant mode. In both cases, red (blue) corresponds to the highest (lowest) intensity.

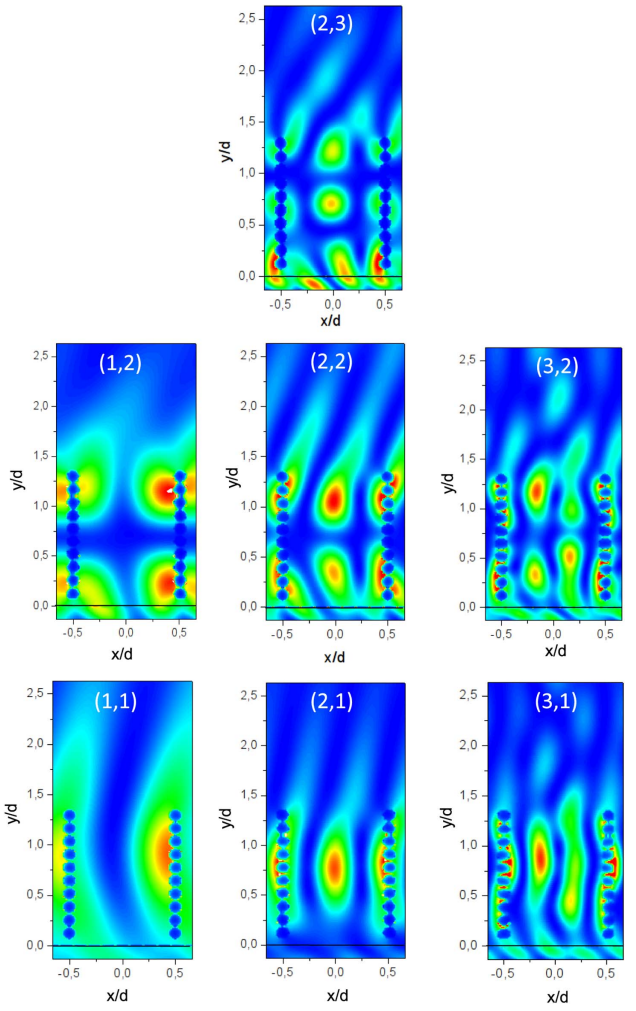

Fig. 4. Near-field intensity maps ($|H|^2$) at the wavelengths corresponding to the peaks observed in the transmission spectrum for 19 cavities [solid line in Fig. 2(b)], at $\lambda/d = 1.777$, 1.25, 0.935, 0.84, 0.71, 0.65, and 0.62. Since $d = 760$ nm, they correspond to $\lambda = 1350.5$, 950.5, 710.6, 638, 539.60, 495, and 471 nm, respectively. The color scales are adapted in each plot in order to highlight the magnetic field distribution of each resonant mode. In all cases, red (blue) corresponds to the highest (lowest) intensity.

at $\lambda/d = 1.777$, 1.25, 0.935, 0.84, 0.71, 0.65, and 0.62. As can be observed, the corresponding maps show well-defined patterns, similar to those obtained for a parallel-plate waveguide. In all cases, intensification of the magnetic field along the chains of metallic cylinders can be noticed, which is accompanied by a decrease in the electric field within the conductor (not shown). The resonant field distributions shown in Fig. 4 can be labeled in the same fashion as those of a rectangular waveguide, i.e., employing indices (i, j), where i and j are positive integers, which denote the number of horizontal and vertical lobes, respectively. Within this framework, these near-field plots are displayed as

$$\begin{bmatrix} & (2,3) & \\ (1,2) & (2,2) & (3,2) \\ (1,1) & (2,1) & (3,1) \end{bmatrix},$$

and these resonant modes are spectrally located at λ/d given by

$$\begin{bmatrix} & (0.71) & \\ (1.25) & (0.84) & (0.62) \\ (1.777) & (0.935) & (0.65) \end{bmatrix}.$$

In Fig. 5, we show near-field intensity maps at the peak wavelengths of the transmission spectrum of a perfectly periodic array of rectangular perfectly conducting wires [see Fig. 2(b)], which are found at $\lambda/d = 1.582$, 1.318, 0.874, 0.772, 0.694, 0.58, and 0.556. As mentioned above, there is a correspondence between the peaks of this curve and those of the transmittance spectrum of the cylinder system [solid curve in Fig. 2(a)]. This correspondence becomes evident when comparing the resonant near-field plots in Fig. 5 with those in Fig. 4. It is clear that the same modes are excited in the perfectly periodic array of rectangular wires, and this confirms that when the cylinders in each chain are sufficiently close to each other, each chain behaves as a solid rectangular wire [30].

It is to expect that as the number of chains increases, the optical response of the whole system tends to that of a perfectly periodic diffraction grating, that is, with discrete well-defined directions for the transmitted power. In such a case, the propagation

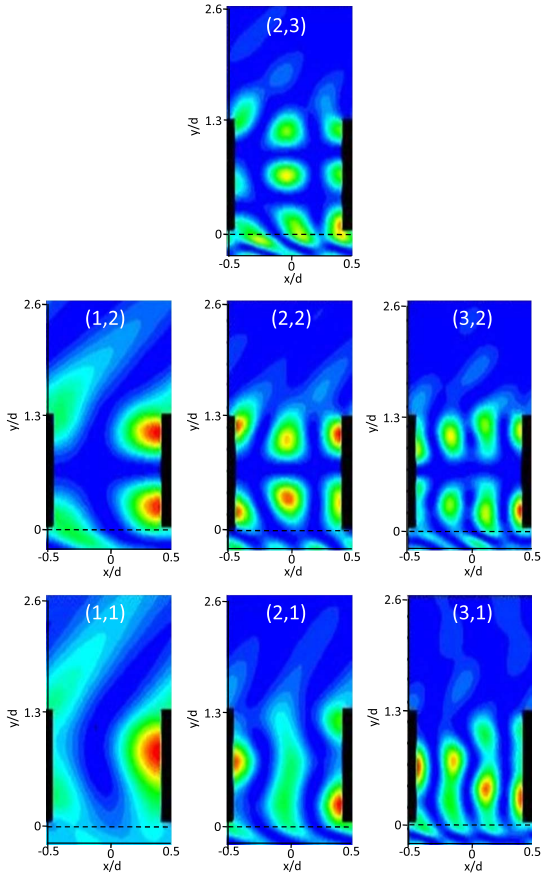

Fig. 5. Near-field intensity maps ($|H|^2$) at the wavelengths corresponding to the peaks observed in the transmission spectrum of a perfectly periodic array of rectangular perfectly conducting wires [see Fig. 2(b)], at $\lambda/d = 1.582$, 1.318, 0.874, 0.772, 0.694, 0.58, and 0.556. The color scales are adapted in each plot in order to highlight the magnetic field distribution of each resonant mode. In all cases, red (blue) corresponds to the highest (lowest) intensity.

directions of the different transmitted orders are given by the grating equation [32]. If the array is illuminated by an evanescent wave, the forward transmitted order (0 order in a diffraction grating) has a grazing direction, i.e., it is parallel to the dielectric interface. The proposed cylinder system placed near the dielectric interface allows us not only to convert the evanescent wave into a propagating wave, but also to optimize the transmitted intensity and to direct it according to the requirements of the specific application. By exciting morphological resonances, it is possible to produce an enhancement of the intensity of the waves transmitted to the far field at directions of diffraction orders other than the zeroth order. For example, as can be observed in Fig. 2(a), at $\lambda/d = 0.84$ (p mode) the total relative transmission is 0.6, 80% of which is directed to the −2 diffraction order. This situation is illustrated in Fig. 6.

Since the resonant modes of the cylinders' structure are related to cavity modes, the optical response is expected to depend on the number of wires in each chain, that is, on the total height h of the array. In Fig. 7(a), we show the evolution of the total transmission (p mode) for the same structure considered in Fig. 2(a) (20 chains, solid line) for different numbers of cylinders in each chain (from 2 to 10), which produce total heights of $h/d = 0.255$, 0.515, 0.775, 1.035, and 1.295. These curves are to be compared with those in Fig. 7(b), which correspond to a perfectly periodic rectangular wire array. Note that the location of the Rayleigh anomalies can be clearly identified in all the curves (vertical dashed lines). As the heights of the chains increase, the transmission curves show more features, associated to the appearance of new cavity modes between the chains of cylinders. The correspondence between the transmission curves for the finite and infinite structures confirms the nature of the resonant mechanism. Maximum transmission is 92%, which occurs for $h/d = 1.035$ (eight cylinders in each chain) at $\lambda/d = 0.91$.

In Fig. 8, we show the near-field intensity map at the resonant condition mentioned above ($h/d = 1.035$, $\lambda/d = 0.91$), and the angular distribution of the transmitted far field (inset).

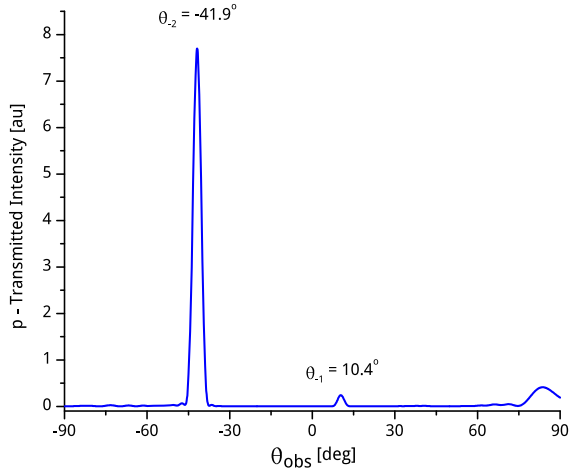

Fig. 6. Angular transmission spectrum at $\lambda/d = 0.84$ for the finite array of 20 Ag subwavelength cylinder chains considered in Fig. 2(a) ($c/d = 0.12$, $a/d = 0.125$, $h/d = 1.295$, $e/d = 0.06$), illuminated by a Gaussian beam of half-width $W/d = 6.6$ ($d = 760$ nm).

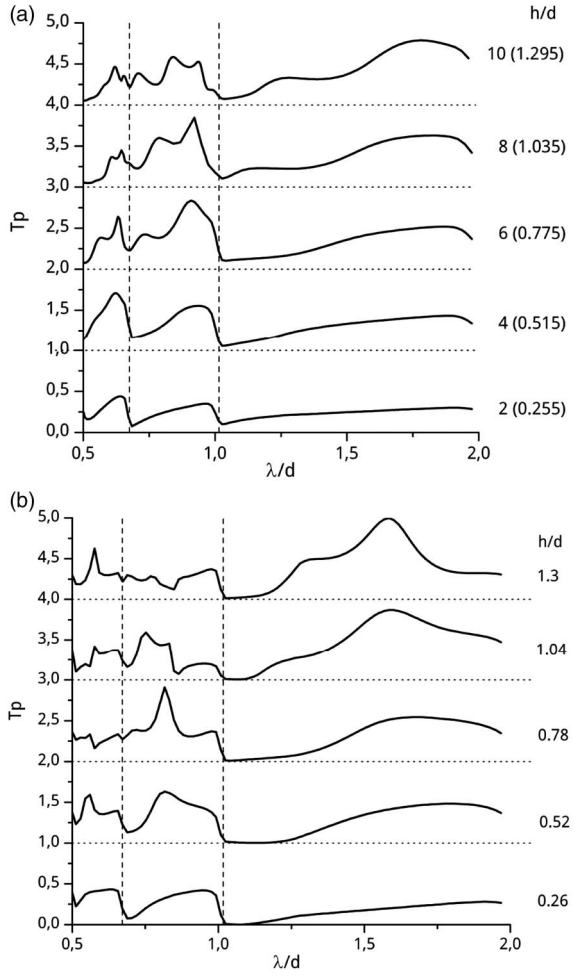

Fig. 7. Total transmission (p mode) for the same system considered in Fig. 2 (solid line), for varying total height of the array. (a) In the case of the finite subwavelength cylinder array, different numbers of cylinders (from 2 to 10) within each chain are considered. (b) In the case of a perfectly periodic rectangular wire array, different values of wire height are considered. The curves are vertically displaced for better visualization. Vertical dashed lines indicate the spectral location of Rayleigh anomalies.

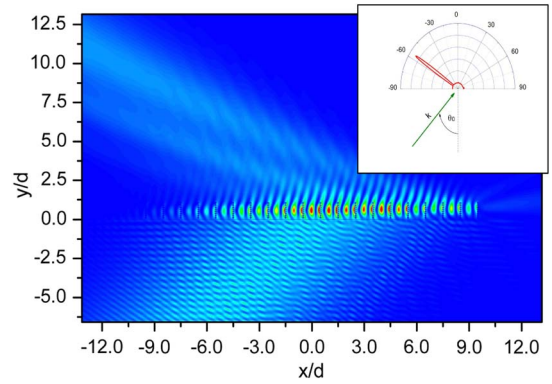

Fig. 8. Near-field intensity map ($|H|^2$) at $\lambda/d = 0.91$ for $h/d = 1.035$ (see Fig. 7). Red (blue) corresponds to the highest (lowest) intensity. Inset: angular transmission spectrum.

The near-field distribution evidences a morphological resonance of type (2,1). Note that more than 90% of the transmitted power propagates in the direction of the −2 order, approximately at an observation angle of −60°. Even though the physical mechanism responsible for redirecting the light beam is grating diffraction, under this resonant condition, the optical behavior of the structure as a whole reminds of the response of a metamaterial of negative refraction index.

Another interesting question that can be asked is how far apart adjacent cylinders can be, while still maintaining the resonant behavior. To address this issue, we computed the far and near fields for structures comprising 6, 8, and 10 cylinders per chain, while keeping the same total height of the structure, i.e., for different distances between adjacent cylinders. These results are shown in Fig. 9. On one hand, note that although the periodicity and total height of the structure are the same for all three cases, the spectral positions of the transmission peaks slightly shift to shorter wavelengths and their transmission intensities decrease as the separation between cylinders increases. This can be explained taking into account that as the cylinders are separated farther from each other, each chain as a whole becomes more permeable to the electromagnetic field, and this modifies the highly conductive boundary condition, which prompts the cavity resonances between the cylinder chains. In other words, the effective dielectric permittivity of each chain becomes less conductive, and this produces a gradual disappearance of the resonant mode. This can be clearly appreciated in the insets in Fig. 9, where we show near-field plots at resonance for the three cases. Note that, as a consequence of the variation of the total transmission, the angular intensity distribution also changes. In all cases, a small peak is observed near $\theta \approx 90°$, which corresponds to the incident grazing wave. Although the directions of the diffraction orders change only slightly—due to a slight shift in the resonant wavelength—the relative intensities change dramatically. Note that in the case of 10 cylinders per chain, the distance between the centers of adjacent cylinders is approximately $\lambda/5$, whereas for the case of six

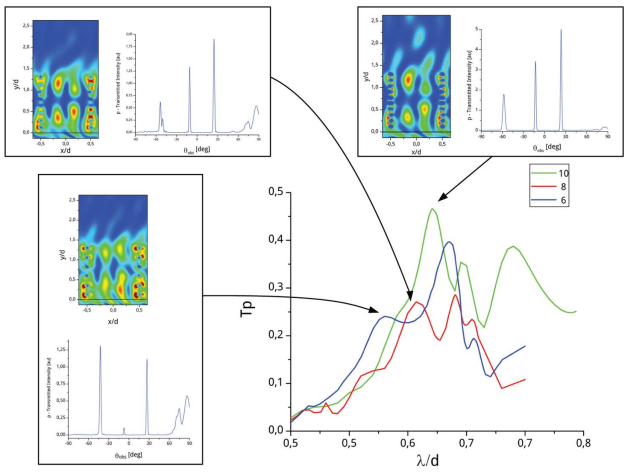

Fig. 9. Total transmission (p mode) for the same system considered in Fig. 2 (solid line), for 6, 8, and 10 cylinders comprising each chain, while keeping the total height of the array fixed at $h/d = 1.295$. Near-field intensity maps ($|H|^2$) at the central cavity and the angular intensity distribution at the resonances are shown as insets.

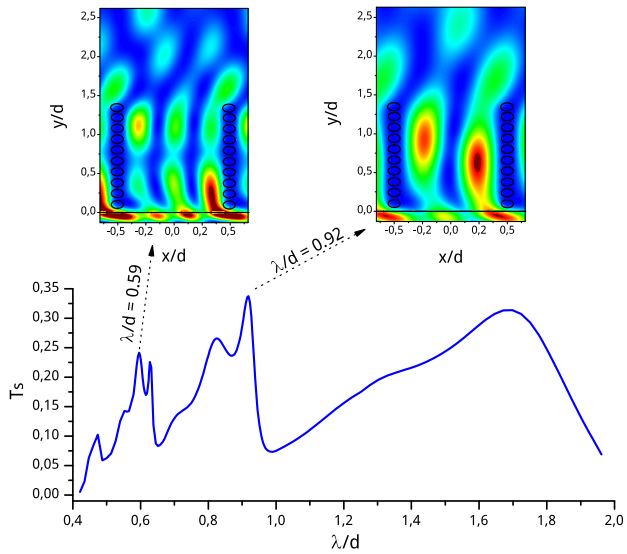

Fig. 10. Total transmission in s mode as a function of wavelength, for the same cylinder structure considered in Fig. 2(a) for 20 chains. Near-field intensity maps ($|E|^2$) at the central cavity at $\lambda/d = 0.59$ and $\lambda/d = 0.92$ are shown as insets. The color scales are adapted in each plot in order to highlight the magnetic field distribution of each resonant mode. In both cases, red (blue) corresponds to the highest (lowest) intensity.

cylinders, it is about $\lambda/3$. Then, it is to expect that the equivalence between a cylinder array and a flat metallic slab would be gradually lost.

For completeness, in Fig. 10 we show the transmitted response of the same 20-cylinder structure considered throughout the paper, but illuminated by an s-polarized beam. The general shape of the curve is quite similar to that for p polarization [Fig. 2(a), solid curve], although the overall intensity is lower than that in the p case. Several peaks can be identified, which can also be associated with morphological resonances. As an example, near-field plots at two of the resonant wavelengths are included as insets in Fig. 10, where typical cavity modes can be appreciated. The near-field map at $\lambda/d = 0.92$ corresponds to a (2,1) mode, whereas that at $\lambda/d = 0.59$ shows a (3,1) mode distribution. Note that, as expected, the electric field vanishes along the metallic cylinder chains. These results suggest that the intensification mechanism is, to some extent, independent of the incident polarization.

4. CONCLUSIONS

This paper theoretically demonstrates resonant optical coupling of a set of cavities illuminated by an evanescent wave, which excites the eigenmodes of the system. Light emission or scattering from objects comprises both propagating and evanescent components, corresponding to low and high wavevectors, respectively. Propagating waves carry large-feature information and reach the far field, whereas evanescent waves contain the information of the details. Since the evanescent components are non-propagating in a usual material environment, they are confined to the near field. In general, the realization of a hyperlens for far-field super-resolution imaging relies on

two basic requirements: a material that supports wave propagation with high wavevectors and a magnification mechanism, that is, conversion of high-wavevector waves to low-wavevector waves so that the super-resolution information can be sent to the far field. We have shown that an evanescent wave can be converted into a propagating wave and, at the same time, the conversion efficiency can be maximized by means of structural resonances, which provide more degrees of freedom for the system design than plasmon resonances. This intensification mechanism is independent of the material of the periodic structure, the incident wavelength, and, to some extent, its polarization. This structure could be employed for super-resolution systems, which rescue the high-resolution information and collect it in the far field. The reported resonances have a morphological origin and, in principle, do not depend on the metal of the cavity walls. The resonant modes follow typical waveguide mode patterns and are robust in the sense that slight variations in the shape of the cavity walls, which could be produced by manufacturing defects, do not significantly alter the excitation of these modes, which occur for both polarization cases. One of the most interesting results is that a high percentage of the transmitted intensity is directed at a well-defined angle and in a direction opposite to the incidence direction. Hence, we have shown that this kind of metastructures formed by optically coupled cavities support eigenmodes similar to those of a waveguide. In addition, the resonant excitation of these morphological eigenmodes allows not only very efficient evanescent-to-propagating conversion for both polarization modes, but also redirection of the transmitted intensity to a particular region of space. This effect resembles that of an antenna array emitting in phase and in directional form. However, further research on the underlying mechanism is still necessary. It is important to remark that the phenomenon reported in this paper does not require a nanometric structure. As long as the metallic cylinders are good conductors, the system is scalable to any region of the electromagnetic spectrum. Therefore, the performance of the system is independent of the typical lengths involved (cylinder radius, total height of the structure, distance between adjacent cylinders, period, etc.), but it only depends on the ratio between these lengths and the incident wavelength. In the nanometer scale, structures similar to the one proposed have been fabricated using inverse techniques or controlled wire growth. For instance, arrays of cylinders on a substrate are being employed for new designs of photoelectric cells or photonic devices [33–35]. Recently, other techniques involving UV radiation have been proposed for the fabrication of nanometric structures, which show even more complexity than those considered in this paper [36,37].

Funding. Universidad de Buenos Aires (UBA) (20020150100028BA); Consejo Nacional de Investigaciones Científicas y Técnicas (CONICET) (PIP 112-201101-00451); Universidad Nacional del Centro de la Provincia de Buenos Aires (UNICEN).

Acknowledgment. D. S. acknowledges partial support from CONICET and UBACyT. M. L. acknowledges partial support from UNICEN.

REFERENCES

1. J. W. Lee, M. A. Seo, D. J. Park, S. C. Jeoung, Q. H. Park, C. Lienau, and D. S. Kim, "Terahertz transparency at Fabry–Perot resonances of periodic slit arrays in a metal plate: experiment and theory," Opt. Express **14**, 12637–12643 (2006).
2. M. R. Gadsdon, I. R. Hooper, and J. R. Sambles, "Optical resonances on sub-wavelength silver lamellar gratings," Opt. Express **16**, 22003–22028 (2008).
3. A. T. M. Anishur Rahman, P. Majewski, and K. Vasilev, "Extraordinary optical transmission: coupling of the Wood–Rayleigh anomaly and the Fabry–Perot resonance," Opt. Lett. **37**, 1742–1744 (2012).
4. S. H. Kim, C. M. Lee, D. W. Park, S. K. Noh, S. B. Sim, J. Kim, G. H. Kim, K. J. Ahn, D. S. Kim, and K. J. Yee, "Evolution of surface plasmon resonance with slab thickness in hybrid nanostructures of Au/InGaAs slab waveguide," Appl. Phys. B **115**, 77–83 (2014).
5. D. C. Skigin and R. A. Depine, "Transmission resonances in metallic compound gratings with subwavelength slits," Phys. Rev. Lett. **95**, 217402 (2005).
6. A. P. Hibbins, I. R. Hooper, M. J. Lockyear, and J. R. Sambles, "Microwave transmission of a compound metal grating," Phys. Rev. Lett. **96**, 257402 (2006).
7. I. Bendoym, A. B. Golovin, and D. T. Crouse, "The light filtering and guiding properties of high finesse resonant compound gratings," Opt. Express **20**, 22830–22846 (2012).
8. H. Lochbihler and R. A. Depine, "Properties of TM resonances on metallic slit gratings," Appl. Opt. **51**, 1729–1741 (2012).
9. F. J. Garca de Abajo, "Colloquium: light scattering by particle and hole arrays," Rev. Mod. Phys. **79**, 1267–1290 (2007).
10. D. M. Natarov, V. O. Byelobrov, R. Sauleau, T. M. Benson, and A. I. Nosich, "Periodicity-induced effects in the scattering and absorption of light by infinite and finite gratings of circular silver nanowires," Opt. Express **19**, 22176–22190 (2011).
11. T. L. Zinenko, M. Marciniak, and A. I. Nosich, "Accurate analysis of light scattering and absorption by an infinite flat grating of thin silver nanostrips in free space using the method of analytical regularization," IEEE J. Sel. Top. Quantum Electron. **19**, 9000108 (2013).
12. H.-T. Chen, A. J. Taylor, and N. Yu, "A review of metasurfaces: physics and applications," Rep. Prog. Phys. **79**, 076401 (2016).
13. Z. Wei, Y. Cao, X. Su, Z. Gong, Y. Long, and H. Li, "Highly efficient beam steering with a transparent metasurface," Opt. Express **21**, 10739–10745 (2013).
14. H. Kurosawa, B. Choi, Y. Sugimoto, and M. Iwanaga, "High-performance metasurface polarizers with extinction ratios exceeding 12000," Opt. Express **25**, 4446–4455 (2017).
15. P. Quemerais, A. Barbara, J. Le Perchec, and T. López-Ríos, "Efficient excitation of cavity resonances of subwavelength metallic gratings," J. Appl. Phys. **97**, 053507 (2005).
16. D. J. Park, S. B. Choi, K. J. Ahn, D. S. Kim, J. H. Kang, Q.-H. Park, M. S. Jeong, and D.-K. Ko, "Experimental verification of surface plasmon amplification on a metallic transmission grating," Phys. Rev. B **77**, 115451 (2008).
17. S. Durant, Z. Liu, J. M. Steele, and X. Zhang, "Theory of the transmission properties of an optical far-field superlens for imaging beyond the diffraction limit," J. Opt. Soc. Am. B **23**, 2383–2392 (2006).
18. X. Hao, C. Kuang, Y. Li, and X. Liu, "Evanescent-wave-induced frequency shift for optical superresolution imaging," Opt. Lett. **38**, 2455–2458 (2013).
19. M. Lester and D. C. Skigin, "Coupling of evanescent s-polarized waves to the far field by waveguide modes in metallic arrays," J. Opt. A **9**, 81–87 (2007).
20. D. C. Skigin and M. Lester, "Enhanced transmission via evanescent-to-propagating conversion in metallic nanoslits: role of Rayleigh anomalies," J. Opt. **16**, 045004 (2014).
21. D. Skigin and M. Lester, "Study of resonant modes of a periodic metallic array near a dielectric interface: evanescent-to-propagating coupling via surface plasmon excitation," J. Opt. A **8**, 259–267 (2006).
22. M. Lester and D. C. Skigin, "An optical nanoantenna made of plasmonic chain resonators," J. Opt. **13**, 035105 (2011).
23. J. A. Porto, F. J. Garca-Vidal, and J. B. Pendry, "Transmission resonances on metallic gratings with very narrow slits," Phys. Rev. Lett. **83**, 2845–2848 (1999).

24. E. Popov, M. Neviére, S. Enoch, and R. Reinisch, "Theory of light transmission through subwavelength periodic hole arrays," Phys. Rev. B **62**, 16100–16108 (2000).
25. S. Astilean, P. Lalanne, and M. Palamaru, "Light transmission through metallic channels much smaller than the wavelength," Opt. Commun. **175**, 265–273 (2000).
26. J. Fiala and I. Richter, "Mechanisms responsible for extraordinary optical transmission through one-dimensional periodic arrays of infinite subwavelength slits: the origin of previous EOT position prediction misinterpretations," Plasmonics (to be published).
27. A. A. Maradudin, T. Michel, A. R. McGurn, and E. R. Mendez, "Enhanced backscattering of light from a random grating," Ann. Phys. **203**, 255–307 (1990).
28. A. Madrazo and M. Nieto-Vesperinas, "Scattering of electromagnetic waves from a cylinder in front of a conducting plane," J. Opt. Soc. Am. A **12**, 1298–1302 (1995).
29. M. Lester, D. C. Skigin, and R. A. Depine, "Control of the diffracted response of wire arrays with double period," Appl. Opt. **47**, 1711–1717 (2008).
30. D. Deslandes and K. Wu, "Single-substrate integration technique of planar circuits and waveguide filters," IEEE Trans. Microwave Theory Tech. **51**, 593–596 (2003).
31. E. Palik, *Handbook of Optical Constants of Solids* (Academic, 1998).
32. R. Petit, *Electromagnetic Theory of Gratings* (Springer-Verlag, 1980).
33. L. Wen, Z. Wang, Y. Mi, R. Xu, S. Yu, and Y. Lei, "Designing heterogeneous 1D nanostructure arrays based on AAO templates for energy applications," Small **11**, 3408–3428 (2015).
34. Q. Xu, R. Perez-Castillejos, Z. Li, and G. M. Whitesides, "Fabrication of high-aspect-ratio metallic nanostructures using nanoskiving," Nano Lett. **6**, 2163–2165 (2006).
35. V. J. Cadarso, N. Chidambaram, L. Jacot-Descombes, and H. Schift, "High-aspect-ratio nanoimprint process chains," Microsyst. Nanoeng. **3**, 17017 (2017).
36. S. Tawfi, M. De Volder, D. Copic, S. J. Park, C. Ryan Oliver, E. S. Polsen, M. J. Roberts, and A. J. Hart, "Engineering of micro- and nanostructured surfaces with anisotropic geometries and properties," IEEE Adv. Mater. **24**, 1628–1674 (2012).
37. L. Romano, J. Vila-Comamala, M. Kagias, K. Vogelsang, H. Schift, M. Stampanoni, and K. Jefimovs, "High aspect ratio metal microcasting by hot embossing for X-ray optics fabrication," Microelectron. Eng. **176**, 6–10 (2017).